

## Rapid Communications

*Rapid Communications are intended for the accelerated publication of important new results and are therefore given priority treatment both in the editorial office and in production. A Rapid Communication in Physical Review B should be no longer than 4 printed pages and must be accompanied by an abstract. Page proofs are sent to authors.*

## Anisotropic optical properties of (110)-oriented quantum wells

D. Gershoni, I. Brener,\* G. A. Baraff, S. N. G. Chu, L. N. Pfeiffer, and K. West

*AT&T Bell Laboratories, Murray Hill, New Jersey 07974*

(Received 4 March 1991)

We present a spectroscopic study of (110)-oriented quantum-well structures. The lower symmetry of the quantum confinement direction that is inherent in these structures results in in-plane polarization anisotropy of the optical transitions. The optical transitions observed in the photoluminescence-excitation spectra of these structures are modeled using an eight-band  $\mathbf{k}\cdot\mathbf{p}$ -type effective-mass theory. We directly determine the valence-band anisotropy of the quantum-well material from the orientational dependence of the transition energies and oscillator strengths.

The spectroscopy of quantum wells (QWs) and superlattices has been intensively investigated since the observation of quantum confinement by optical means.<sup>1</sup> Most of these investigations have been performed on (100)-oriented structures, since high-quality epitaxial growth was traditionally available in this crystallographic orientation only.<sup>2-4</sup> In order to account for the detailed spectroscopic studies of QW structures which followed the observation by Dingle and co-workers,<sup>1</sup> several theoretical models have been developed,<sup>5-10</sup> far more complicated than the intuitive "particle-in-a-box" description.<sup>1</sup> From these models it became clear that the wave functions and consequently the optical properties of these quantum-confined systems should be sensitive to the crystallographic direction of the epitaxial growth. This is mainly due to the valence-band anisotropy of the zinc-blende III-V binary compounds used for the heteroepitaxy. Recently, there have been a few studies of heterostructures with nonconventional crystallographic orientations.<sup>11-13</sup> In these studies it has been experimentally shown that, indeed, both the energies and the oscillator strengths of the interband optical transitions are sensitive to the crystallographic direction of the epitaxial growth.

In this work, we report on detailed spectroscopic studies of single-QW structure formed by high-quality epitaxial growth on a (110)-oriented substrate.<sup>14,15</sup> We show, both experimentally and theoretically, that the lower symmetry of the composition-induced quantum confinement [(110) here as opposed to (100) or (111) studied previously] results in an in-plane polarization anisotropy of the spectral response of the sample. Our eight-band  $\mathbf{k}\cdot\mathbf{p}$  model accurately describes the optical transition energies as well as their polarization anisotropy up to 250 meV above the QW band gap (this is somewhat surprising, since the model does not explicitly contain the  $L$  and  $X$  bands). From the observed optical anisotropies, we can thus quite accurately determine the valence-band anisotropy of GaAs—the QW material.

The  $\text{Al}_{0.26}\text{Ga}_{0.74}\text{As}/\text{GaAs}$  multiple-quantum-well (MQW) samples were grown by molecular-beam epitaxy (MBE) simultaneously on two different GaAs wafers. One was (100) oriented and the other one was (110) oriented, both to within a tenth of a degree. During growth the wafer temperature was 480°C as measured by an infrared pyrometer and the  $\text{As}_4$  partial pressure was  $1.6\times 10^{-5}$  torr measured at the substrate position. The rate of growth of GaAs under these conditions was 0.5  $\mu\text{m}/\text{h}$ , and a smooth featureless morphology was obtained on both substrates. Modulation-doped 250-Å-wide QWs grown in the same conditions show two-dimensional electron-gas mobilities as high as  $5\times 10^5$   $\text{cm}^2/\text{Vs}$  for the (110)-oriented substrate and about a factor of 3 lower for the (100)-oriented one. A very thin GaAs buffer layer ( $\sim 30$  Å) was deposited prior to the growth of three GaAs QWs of different widths, separated by 150–200-Å-thick  $\text{Al}_{0.26}\text{Ga}_{0.74}\text{As}$  barriers. The samples were not rotated during growth so thickness gradients of about 7 percent per cm resulting from differences in distance from the effusion cells are expected. To circumvent the difficulty of well size determination, we used cross-section transmission electron microscopy (TEM) to determine the dimensions of the QWs in the exact positions where the optical studies had been carried out. The exact aluminum concentration was then determined from the optical spectroscopy within the uncertainties of the nominal growth value. Figure 1 shows dark field TEM micrographs of the cross-sectional view of (a) the (110) sample using (220) reflection, and (b) the (100) sample using (200) reflection. Both reflections had the  $\mathbf{g}$  (diffraction) vector perpendicular to the interfaces of the structures, and were found to give sharp contrast of the interfaces. Note the difference in the background contrast of the  $\text{Al}_x\text{Ga}_{1-x}\text{As}$  barriers between Figs. 1(a) and 1(b). In the (110)-oriented sample [Fig. 1(a)] a fine line structure perpendicular to the growth direction is observed. Similar structures have been reported before for growth directions which are slightly

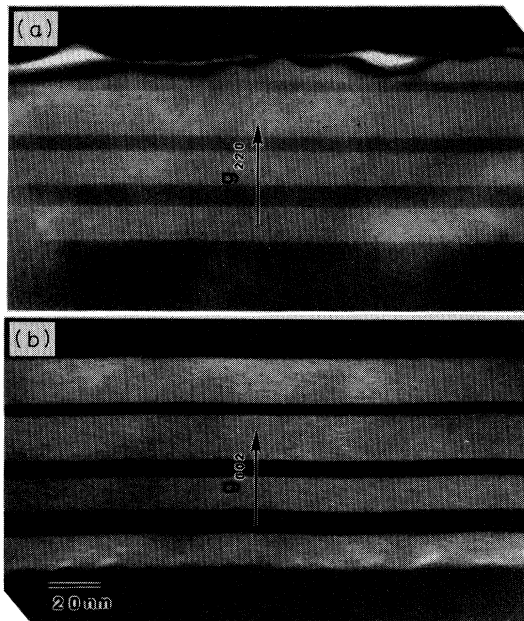


FIG. 1. Dark field reflection TEM micrograph of (a) (110)-oriented MQW sample, and (b) (100)-oriented MQW sample.

off the (110) direction.<sup>16,17</sup> They were attributed to short-range atomic ordering typical of epitaxial growth in this crystallographic direction.<sup>17</sup> The effect that we observe is much smaller, probably due to the lower aluminum atomic mobility at our much lower growth temperature.

For the photoluminescence (PL) and PL excitation (PLE) measurements the samples were oriented using two cleavage planes and placed in a He-flow cryostat. A pyridin-2 dye laser pumped by an Ar<sup>+</sup> ion laser was used as a continuously tunable source of excitation. The laser light was focused at normal incidence onto the sample surface and its polarization was controlled by a polarization plane rotator and a polarizer. The luminescence from the sample was collected at a large solid angle perpendicular to the exciting light direction (see inset to Fig. 2). The PL, collected this way from both samples, was found to be completely unpolarized.

Figure 2 displays a set of PL spectra from the (110)-oriented sample for various polarization angles of the exciting laser light measured from the  $[\bar{1}10]$  crystallographic direction. The spectra that were excited at 1.746 eV show a clear polarization angle dependence of the emission intensity from the three QWs. In contrast, the two lowest energy lines, which originated in the GaAs substrate, do not show this dependence. At this particular excitation energy the emissions from the narrowest and from the widest QWs have a similar dependence on the polarization angle. Both have a clear maximum (minimum) when the light is polarized along the [001] ( $[\bar{1}10]$ ) crystallographic direction. The emission intensity from the middle size well shows the opposite dependence. It reaches maximum (minimum) when the polarization is parallel to the  $[\bar{1}10]$  ([001]) axis. In a similar study we found that the PL intensity from all the (100)-oriented

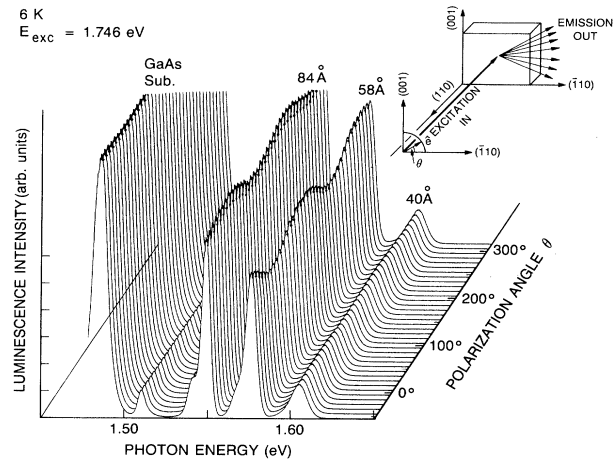


FIG. 2. PL spectra of the (110)-oriented MQW structure for various excitation polarization angles  $\theta$  measured from the  $[\bar{1}10]$  crystallographic axis (see inset).

QWs was completely polarization independent.

This unusual behavior of the PL from (110)-oriented QWs is described more completely in Fig. 3(a). The figure displays the PL spectrum (lowest solid line), the  $[\bar{1}10]$  polarized PLE spectra (solid lines), and the [001] polarized PLE spectra (dashed lines) from the three (110)-oriented QWs. The PLE spectra are vertically displaced for clarity. The energy of excitation for which Fig. 2 was obtained is marked with an arrow in Fig. 3(a). In Fig. 3(c) we show the PLE spectra from the three QWs in the (100)-oriented sample. Since no polarization dependence was observed here, there is only one (solid) line for each PLE spectrum.

The calculated absorption spectra for the (110)  $[\bar{1}10]$ -oriented QWs are shown for comparison in Fig. 3(b) [Fig. 3(d)]. Our model for calculating absorption spectra does not include excitonic effects, therefore the spectra are down shifted by 0.01 eV to roughly account for the two-dimensional exciton binding energy. The experimental PLE spectra are dominated by excitonic resonances, thus the similarity between them and the calculated absorption is not immediately evident. However, if those resonances are ignored, the agreement is quite satisfactory. The polarization anisotropy and the peak energies (to within the experimental linewidths) are both very well described by our calculations for all six QWs.

Our absorption calculations proceed along the lines described in Ref. 10. We use a Fourier expansion method to solve the eight-band  $\mathbf{k}\cdot\mathbf{p}$  Kane-Luttinger Hamiltonian with bulk parameters for each material region. This converts the coupled differential equations into a matrix eigenvalue problem, which is then solved numerically. The discontinuity in the material parameters is taken care of by a procedure discussed in Ref. 10. This procedure, which tremendously simplifies the formulation of the problem, and which is easily generalized to problems in two and three dimensions, is equivalent to the usual condition that the normal component of the probability current be continuous across internal interfaces. The method can

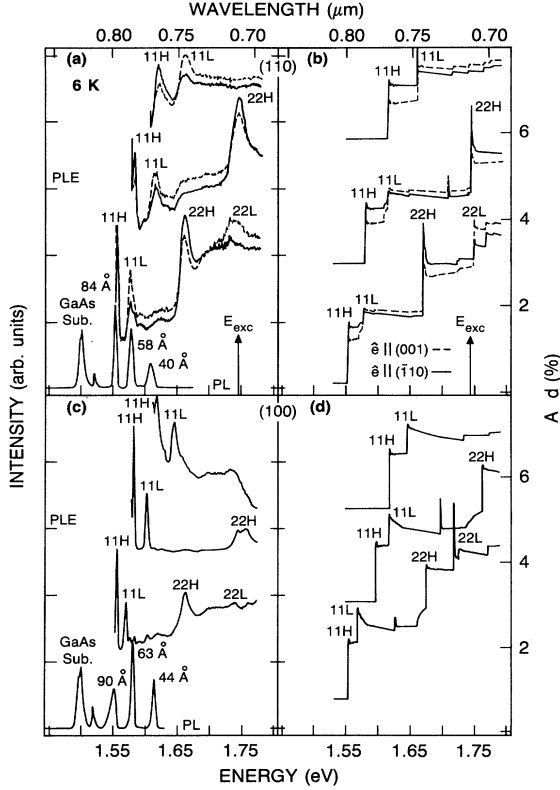


FIG. 3. (a) [(c)] Measured and (b) [(d)] calculated PLE spectra of the (110) [(100)]-oriented MQW sample. The calculated and measured PLE spectra are vertically displaced above the measured PL spectra which are also shown (lowest solid line).

be applied to an arbitrary crystallographic direction of composition-induced confinement by a simple rotation of the differential operators.

The calculation of the absorption spectrum was not discussed in Ref. 10; we describe it here in some detail. In the situation where the direction perpendicular to the quantum well is (say)  $\hat{z}$  and the system is uniform and infinite in the (say)  $\hat{x}$  and  $\hat{y}$  directions, the individual states  $\Psi_i(\mathbf{k}_{\parallel}, z)$  and the individual energies  $E_i(\mathbf{k}_{\parallel})$  are la-

beled by the quantum number  $i$  (for the different bands and due to quantization along the  $\hat{z}$  direction) and the in-plane wave vector  $\mathbf{k}_{\parallel}$  (with components  $k_x$  and  $k_y$ ). After the states and energies have been calculated via the method described in Ref. 10, it is straightforward to evaluate the optical matrix element  $M_{ij}(\mathbf{k}_{\parallel})$  for transitions between states  $i$  and  $j$ ,

$$M_{ij}(\mathbf{k}_{\parallel}) = |\langle \Psi_i(\mathbf{k}_{\parallel}) | \hat{\mathbf{e}} \cdot \frac{\hbar}{i} \nabla | \Psi_j(\mathbf{k}_{\parallel}) \rangle|^2, \quad (1)$$

where  $\hat{\mathbf{e}}$  is a unit vector in the direction of the electric field associated with the optical radiation. The absorption coefficient ( $A$ ) for a given photon frequency ( $\omega$ ) is then given by

$$A(\hbar\omega) = \frac{4\pi^2 \hbar^2 \alpha}{ndm^2(\hbar\omega)} \sum_{i,j} \int M_{ij}(\mathbf{k}_{\parallel}) d\mathbf{k}_{\parallel} \times \delta[E_i(\mathbf{k}_{\parallel}) - E_j(\mathbf{k}_{\parallel}) - \hbar\omega]. \quad (2)$$

Here  $\alpha$  is the fine structure constant,  $n$  is the index of refraction,  $m$  is the electron mass, and  $d$  is the quantum-well width. The two-dimensional integral over the in-plane wave vector in Eq. (2) can be conveniently expressed as a one-dimensional integral,<sup>18</sup>

$$\int M_{ij}(\mathbf{k}_{\parallel}) d\mathbf{k}_{\parallel} \delta[E_i(\mathbf{k}_{\parallel}) - E_j(\mathbf{k}_{\parallel}) - \hbar\omega] = \int_0^{2\pi} d\phi \frac{k M_{ij}(k, \phi)}{\partial E_{ij}(k, \phi) / \partial k}. \quad (3)$$

In Eq. (3),  $k$  is the norm of the in-plane wave vector  $\mathbf{k}_{\parallel}$ ,  $\phi$  is its azimuthal angle, conveniently measured from the electric-field direction  $\hat{\mathbf{e}}$ , and  $E_{ij}(k, \phi) = E_i(k, \phi) - E_j(k, \phi)$ .

To calculate the integral in the right-hand side of Eq. (3), we evaluate the integrand for evenly spaced values of  $\phi$ , average the results, and multiply by  $2\pi$ . In practice, the process converges well for a very small number of divisions of the interval  $2\pi$ . Moreover, we have found that for the case of quantum confinement along the principal crystallographic axis [100] and polarization field along a principal crystallographic axis in the QW plane, such as [010], this average is given exactly by evaluating at the

TABLE I. Parameters used in calculations.

	$E_g$ (eV)	$\Delta_{so}$ (eV)	$\gamma_1$	$\gamma_2$	$\gamma_3$	$2mP^2/\hbar^2$ (eV)	$m_c^*$ (e.m.u)	Valence-band offset (eV)
GaAs	1.519 <sup>a</sup>	0.340 <sup>a</sup>	6.790 <sup>b</sup>	1.924 <sup>b</sup>	2.782 <sup>c</sup>	28.8 <sup>d</sup>	0.0665 <sup>a</sup>	0.0
Al <sub>0.26</sub> Ga <sub>0.74</sub> As	1.845 <sup>e</sup>	0.323 <sup>f</sup>	6.942 <sup>g</sup>	1.658 <sup>g</sup>	2.838 <sup>c</sup>	27.0 <sup>f</sup>	0.089 <sup>f</sup>	-0.131 <sup>h</sup>

<sup>a</sup>Semiconductors, edited by O Madelung, M. Schulz, and H. Weiss, Landolt-Börnstein, New Series Group 3 Vol. 17A (Springer, Berlin, 1982).

<sup>b</sup>Reference 4.

<sup>c</sup>Best fit to our optical data.

<sup>d</sup>C. Hermann and C. Weisbuch, Phys. Rev. B **15**, 823 (1977); C. Weisbuch and C. Hermann, *ibid.* **15**, 826 (1977).

<sup>e</sup>We use AlAs direct band gap of 3.04 eV and a bowing parameter of 0.37 eV.

<sup>f</sup>We use linear interpolation between the binary values as given in footnote a.

<sup>g</sup>We use linear interpolation between the effective masses in the [100] crystallographic direction as given in footnote a.

<sup>h</sup>Following Ref. 4 we assume that 40% of the band-gap discontinuity takes place in the valence band.

single point  $\phi = \pi/4$ . This yields the well-known result that the in-plane absorption of a (100) QW is completely unpolarized. Similarly, we have observed that evaluating at  $\phi = \pi/4$  results in a very good approximation for the average over all the azimuthal intervals for the case of the (110)-oriented QW with polarization field along the  $[\bar{1}10]$  or  $[001]$  crystallographic directions in the QW plane. Figures 3(c) and 3(d) were calculated by using  $\phi = \pi/4$  in the evaluation of the integral in Eq. (3). The material parameters used in these calculations are listed and referenced in Table I.

A word of caution is due here; a few of the parameters are not very well determined yet, in particular, those of the  $\text{Al}_x\text{Ga}_{1-x}\text{As}$  ternary barrier. Fortunately, the calculations are not too sensitive to the values of the barrier's band structure  $\gamma_i$  and  $P$  parameters (where  $\gamma_i$ ,  $i=1,2,3$  are the Luttinger parameters,<sup>19</sup> and  $P$  is the conduction-valence-band interaction matrix element.) The computed spectra are much more sensitive to the band-structure parameters of the QW material. We were able to compute spectra, all of which equally resembled the experimental results using different combinations of those  $\gamma_i$  and  $P$  parameters. We found, however, that the quality of the fit to

both the transition energies and polarization anisotropies is a very sensitive function of the valence-band anisotropy of the QW material which we define as  $\gamma_a = (\gamma_3 - \gamma_2)/(\gamma_3 + \gamma_2)$ . Since our goal was to experimentally estimate the valence-band anisotropy, we chose accepted parameters (except  $\gamma_3$ ) from the literature. We obtained  $\gamma_3$  from the best simultaneous fits to the six different PLE spectra in Fig. 3(a). Thus, comparison between the computed spectra and the experimental measurements provides an all-optical method of measuring this otherwise difficult to determine parameter. We obtained Figs. 3(b) and 3(d) [which best agree with Figs. 3(a) and 3(c)] using  $\gamma_a = 0.18 \pm 0.03$ . This value is in close agreement with other experimental determinations, with<sup>20</sup> and without<sup>11-13</sup> magnetic field. This value is quite far, however, from some theoretical calculations<sup>21</sup> which have been extensively used for modeling QWs in this material system.

In summary, we report on optical spectroscopy of (110)-oriented quantum wells. We account for both the energies and oscillator strengths of all the observed interband transitions in terms of an eight-band  $\mathbf{k} \cdot \mathbf{p}$  effective-mass theory. We used our results to independently determine the valence-band anisotropy in GaAs.

\*Present address: Physics Department, Technion, Haifa 32000, Israel.

<sup>1</sup>R. Dingle, W. Wiegmann, and C. H. Henry, Phys. Rev. Lett. **33**, 827 (1974).

<sup>2</sup>R. C. Miller, D. A. Kleinman, W. A. Nordland, and A. C. Gossard, Phys. Rev. B **22**, 863 (1980).

<sup>3</sup>R. C. Miller, D. A. Kleinman, and A. C. Gossard, Phys. Rev. B **29**, 7085 (1984).

<sup>4</sup>D. F. Nelson, R. C. Miller, and D. A. Kleinman, Phys. Rev. B **35**, 7770 (1987).

<sup>5</sup>L. J. Sham and M. Nakayama, Phys. Rev. B **20**, 734 (1979).

<sup>6</sup>G. Bastard, Phys. Rev. B **24**, 5693 (1981); **25**, 7584 (1982).

<sup>7</sup>M. Altarelli, Phys. Rev. B **28**, 842 (1983).

<sup>8</sup>J. N. Schulman and Y. C. Chang, Phys. Rev. B **31**, 2056 (1985).

<sup>9</sup>R. Eppenga, M. F. Schuurmans, and S. Colak, Phys. Rev. B **36**, 1554 (1987).

<sup>10</sup>G. A. Baraff and D. Gershoni, Phys. Rev. B **43**, 4011 (1991).

<sup>11</sup>T. Hayakawa, T. Suyama, K. Takahashi, M. Kondo, T. Suyama, S. Yamamoto, and T. Hijikata, Phys. Rev. Lett. **60**, 349

(1988).

<sup>12</sup>L. W. Molenkamp, R. Eppenga, G. W. 't Hooft, P. Dawson, C. T. Foxon, and K. J. Moore, Phys. Rev. B **38**, 4314 (1988).

<sup>13</sup>B. V. Shanabrook, O. J. Glembocki, and D. A. Broido, Phys. Rev. B **39**, 3411 (1989).

<sup>14</sup>L. N. Pfeiffer, K. W. West, H. L. Stormer, J. Eisenstein, K. W. Baldwin, D. Gershoni, and J. Spector, Appl. Phys. Lett. **56**, 1697 (1990).

<sup>15</sup>D. Gershoni, J. S. Weiner, S. N. G. Chu, G. A. Baraff, J. M. Vandenberg, L. N. Pfeiffer, K. West, R. A. Logan, and T. Tanbun-Ek, Phys. Rev. Lett. **65**, 1631 (1990).

<sup>16</sup>P. M. Petroff, A. Y. Cho, F. K. Reinhart, A. C. Gossard, and W. Wiegmann, Phys. Rev. Lett. **48**, 170 (1982).

<sup>17</sup>T. S. Kuan, T. F. Kuech, W. I. Wang, and E. L. Wilkie, Phys. Rev. Lett. **54**, 201 (1985).

<sup>18</sup>G. A. Baraff and D. Gershoni (unpublished).

<sup>19</sup>J. M. Luttinger, Phys. Rev. **102**, 1030 (1956).

<sup>20</sup>M. S. Skolnick, A. K. Jain, R. A. Stradling, J. Leotin, J. C. Ousset, and S. Askenazy, J. Phys. C **9**, 2809 (1976).

<sup>21</sup>P. Lawaetz, Phys. Rev. B **4**, 3460 (1971).

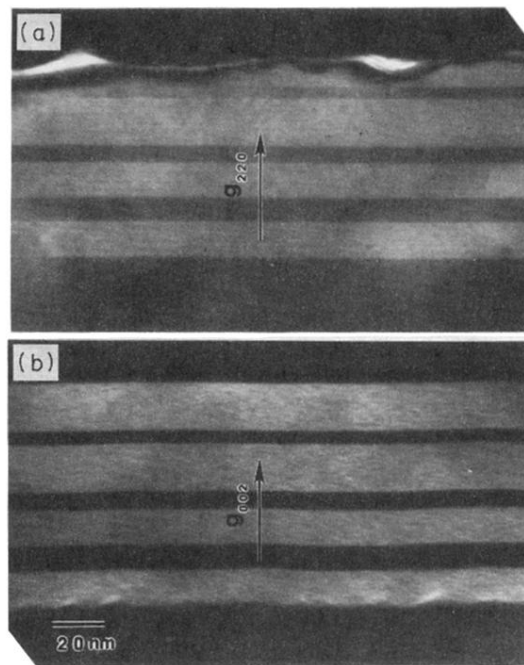


FIG. 1. Dark field reflection TEM micrograph of (a) (110)-oriented MQW sample, and (b) (100)-oriented MQW sample.